Real-Time Observation of the Solid–Liquid–Vapor Dissolution of Individual Tin(IV) Oxide Nanowires

Bethany M. Hudak,[†] Yao-Jen Chang,[†] Lei Yu,[†] Guohua Li,[†] Danielle N. Edwards,[†] and Beth S. Guiton[†,‡,*]

[†]Department of Chemistry, University of Kentucky, Lexington, Kentucky 40506, United States and [‡]Materials Science and Technology Division, Oak Ridge National Laboratory, Oak Ridge, Tennessee 37831, United States

ABSTRACT The well-known vapor–liquid–solid (VLS) mechanism results in high-purity, single-crystalline wires with few defects and controllable diameters, and is the method of choice for the growth of nanowires for a vast array of nanoelectronic devices. It is of utmost importance, therefore, to understand how such wires interact with metallic interconnects—an understanding which relies on comprehensive knowledge of the initial growth process, in which a crystalline wire is ejected from a metallic particle. Though ubiquitous, even in the case of single elemental nanowires the VLS mechanism is complicated by competing processes at multiple heterogeneous interfaces, and despite decades of study, there are still aspects of the mechanism which are not well understood. Recent breakthroughs in studying the mechanism and kinetics of VLS growth have been strongly aided by the use of *in situ* techniques, and would have been impossible through other means. As well as several systematic studies of nanowire growth, reports which focus on the role and the nature of the catalyst tip reveal that the stability of the droplet is a crucial factor in determining nanowire morphology and crystallinity. Additionally, a reverse of the VLS process dubbed solid–liquid–vapor (SLV) has been found to result in the formation of cavities, or "negative nanowires". Here, we present a series of heating studies conducted *in situ* in the transmission electron microscope (TEM), in which we observe the complete dissolution of metal oxide nanowires into the metal catalyst particles at their tips. We are able to consistently explain our observations using a solid–liquid–vapor (SLV) type mechanism in which both evaporation at the liquid–vapor interface and adhesion of the catalyst droplet to the substrate surface contribute to the overall rate.

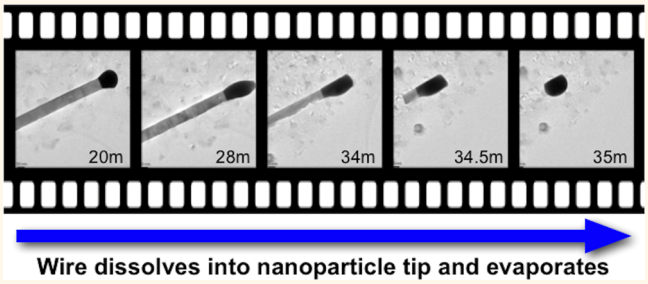

KEYWORDS: vapor–liquid–solid (VLS) · solid–liquid–vapor (SLV) · nanowire · *in situ* TEM · semiconductor · nanoelectronics · rutile · tin dioxide

The vapor–liquid–solid (VLS) nanowire growth technique is the method of choice for the synthesis of a vast range of single-crystalline nanowires for equally numerous uses.[1−3] VLS synthesis is well-known to be the most effective method of controlling nanowire diameter during nanowire growth, *via* the size of the metal catalyst particle,[3] and results in wires with easily controlled lengths and high-crystallinity. SnO_2 is an n-type semiconductor with a wide band gap (3.6 eV at 300 K) and is easily grown in a nanowire morphology using the VLS synthesis. These semiconducting nanowires are building blocks for nanoscale electronics and optoelectronic devices with specific applications to gas sensors,[4−6] dye sensitized solar cells,[7−9] field-effect transistor devices,[10,11] and Li-ion batteries.[12,13] For use in these kinds of devices, nanowires need to be stable at high temperatures and when in contact with metals.[14,15] In addition to pure SnO_2, there is much interest in the Sn-rich end of the SnO_2–In_2O_3 solid solution, for applications such as enhancing the selectivity of SnO_2 gas sensors;[15−17] the operating temperatures for both doped and pure SnO_2 gas sensors can reach 200–500 °C.[15] Though many gas sensing devices are built from thin films,[15−17] replacing these with 1D nanostructures can increase their performance due to the increased surface area, aspect ratio, and crystallinity associated with 1D nanostructures.[18,19] It is therefore imperative to understand the behavior of both pure and doped-SnO_2 nanowires at elevated temperatures, and in particular the way in which

* Address correspondence to beth.guiton@uky.edu.

Received for review June 17, 2013 and accepted May 12, 2014.

Published online May 13, 2014
10.1021/nn5007804

© 2014 American Chemical Society

these nanowires interact with the gold and other metallic connecting materials. For these reasons, we have undertaken a series of *in situ* heating experiments in which we examine the interaction of SnO_2 nanowires with the metal catalyst particle, which is residual at the tip of the wire after VLS synthesis. Our observations should be generalizable to other metal oxide nanowire materials and of relevance to all VLS-grown nanowire systems.

VLS growth is the key mechanism of silicon nanowire growth, and as such has been studied extensively to elucidate the key mechanistic processes and kinetics. The growth process can be divided into three main steps:[20,21] first, a silicon containing precursor is cracked at the surface of a liquid catalyst droplet, usually gold, and silicon is incorporated into the catalyst. In the second step, Si quickly diffuses through the droplet to (what will become) the solid–liquid interface, and the droplet supersaturates with Si. At sufficient supersaturation, Si crystallizes out in the third step of the mechanism to form a nanowire whose diameter depends on the initial droplet size. In the limiting case that only one of these steps is rate-determining, the growth velocity of the wire, d*L*/d*t*, may or may not depend on wire diameter. If crystallization is the only rate-determining step, the Gibbs–Thomson effect dictates that d*L*/d*t* is inversely proportional to negative wire diameter, so that larger wires grow more quickly. This was the situation described by Givargizov.[22] If incorporation is instead the rate-determining step, d*L*/d*t* is independent of nanowire diameter, but will depend on the partial pressure of the precursor vapor, as was observed by Kodambaka *et al.*[23] It is possible, however, for the actual situation to lie between these two limits, with the rate of growth determined by the interplay between these steps.[20,21] Additionally, several reports in the theoretical literature[24–26] predict that nanowire growth relies on a steady-state balancing of the nanowire crystallization, with melting or dissolution back into the catalyst, and that it is important to understand both processes, since they rely on different morphological features.

Given the dependence of kinetics on the balancing of several steps, and that wire diameters can vary during growth, understanding the kinetics of growth has been greatly advanced by the real-time observation of nanowire growth *in situ* in the transmission electron microscope (TEM).[2,23] Recent observations of both the growth of nanowires by the VLS mechanism and also their subsequent annealing have revealed some fascinating behavior of the metal droplet at the tip of the wire. Hannon *et al.* observed that the catalyst droplets actually change during growth, and that diffusion of Au down the sidewalls of the growing nanowires and across the substrate can result in Ostwald ripening of the droplets, and a resulting tapering of nanowire diameter.[27] This is consistent with an observation by Sutter and Sutter that traces of Au remain on the sidewalls of Ge nanowires after VLS synthesis, and can be used to catalyze the encapsulation of the nanowire in a graphitic coating.[28] Sutter and Sutter also observed the melting and recrystallization of alloy particles at the tips of germanium and GaAs nanowires to find a strong size dependence of the alloy composition, which allowed a tunable depression of the liquidus.[29–31] Finally, metal droplets have also been reported to catalyze a reverse process of the VLS mechanism, dubbed solid–liquid–vapor (SLV), in which the droplet etches a cavity or tunnel in a soluble material to form negative nanowires or whiskers.[32,33]

Here, we use *in situ* heating in the TEM to observe the kinetics of gold-catalyzed dissolution of SnO_2 nanowires with the rutile structure. Observing this process *in situ* provides physical insight into the mechanism, which suggests that both overcoming adhesion of the Au alloyed droplet to the substrate surface and evaporation at the liquid–vapor interface are likely to be key rate-determining steps.

RESULTS AND DISCUSSION

We conducted *in situ* heating experiments in which we anneal SnO_2 and In-doped SnO_2 nanowires in the TEM, and observe etching of the nanowires by the Au catalyst droplet at their tips. This dissolution process is consistently reproducible under conditions of elevated temperature in the low pressure TEM environment, provided that the wire remains in contact with its gold catalyst head. It can be controlled, stopped, and started by altering the temperature, in many cases eventually leading to complete dissolution of the wire leaving nothing remaining but the original metal catalyst particle. The nanowires for this study were synthesized by a standard VLS growth method, to obtain single-crystalline wires with a wide range of diameters from ~20 to 300 nm and lengths varying from several hundreds of nanometers to tens of micrometers. A high resolution high angle annular dark field (HAADF) scanning TEM image of the Au/SnO_2 interface from a typical nanowire is displayed in Figure S1 showing the [101] growth direction typical for these wires. X-ray diffraction (XRD) patterns from both pure and In-doped SnO_2 wires are also shown in Figure S1, and in both cases can be indexed to the rutile phase of SnO_2.

To investigate the behavior of our wires at elevated temperature, we imaged individual VLS-grown wires deposited on a heating substrate (Protochips E-chip) and heated to temperatures in the *in situ* holder in the range of 400–800 °C, such that etching was observed. Shown in Figure 1 are representative frames from movies taken from five different wires within the SnO_2–In_2O_3 solid solution. At temperatures greater than 450 °C, the gold catalyst particle is seen to

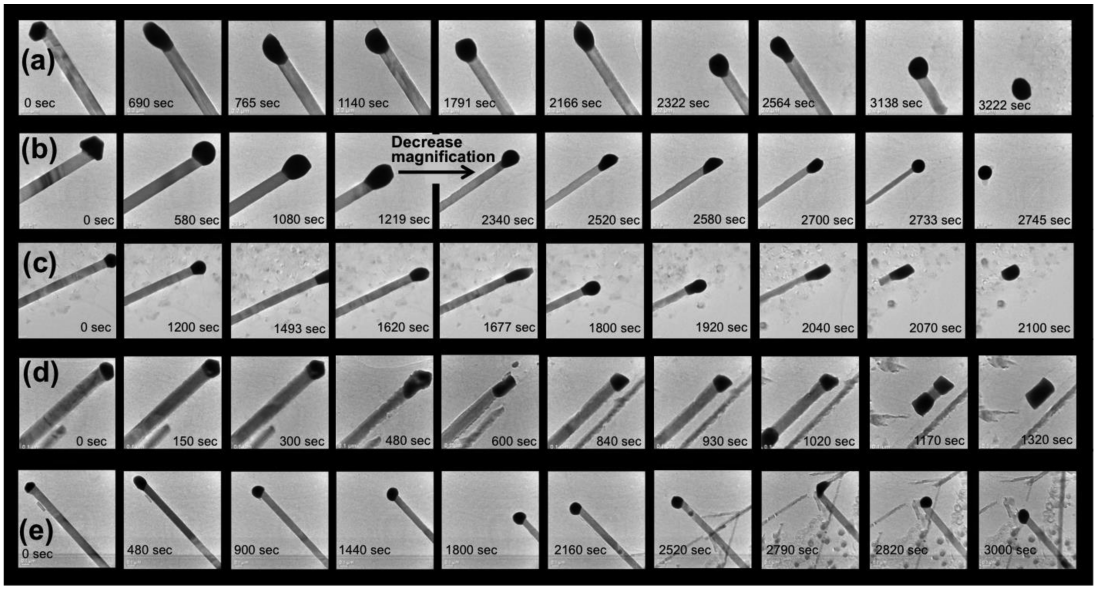

Figure 1. Representative frames from five movies of nanowire heating experiments (corresponding to Movies S1−S5). (a) A pure SnO_2 nanowire is seen to dissolve into the gold catalyst particle at its head. Field of view is 1.13 μm. (b) A pure SnO_2 nanowire dissolves into the gold catalyst while the diameter of the wire simultaneously decreases. Field of view is 870 nm, and then increases to 1.10 μm when the magnification decreases. (c) An In-doped SnO_2 wire is seen to dissolve into the gold particle at its head. Field of view is 870 nm. (d) An In-doped SnO_2 nanowire is seen to dissolve simultaneously into gold particles at either end of the wire. Field of view is 730 nm. (e) An In-doped SnO_2 nanowire dissolves into the gold catalyst, and starts to change direction part way. Field of view is 1.10 μm.

consume the entire length of these rutile-type nanowires, with what appears to be a reverse of the standard VLS mechanism. In every wire studied, dissolution of the wire is preceded by a loss of faceting in the gold catalyst head, indicating that melting of the tip is a necessary first step. This is especially apparent in the first two panels of Figure 1b. The subsequent motion of the tip (Movies S1−S5) also suggests a fluid-like behavior. Details of the temperature profiles used to heat these wires are given in the Supporting Information movie files, Movies S1−S5.

In Figure 1a, the gold catalyst particle migrates down the entire length of a pure-SnO_2 nanowire, consuming the wire over the space of ~54 min, until a stationary, isolated nanoparticle remains. In Figure 1b, the catalyst particle again consumes the entire length of a pure-SnO_2 nanowire, accompanied in this case by a simultaneous reduction in wire diameter. Similar observations were recorded for In-doped SnO_2 nanowires, and are shown in Figure 1c−e, demonstrating that this phenomenon is generally applicable into the solid solution. Figure 1c shows an In-doped SnO_2 wire in which a mechanism similar to that of Figure 1a is observed; the nanoparticle migrates the length of the wire resulting in a stationary, isolated nanoparticle. Figure 1d shows the effect of putting a wire in contact with multiple gold particles; toward the end of the recording, a second catalyst particle appears in the bottom of the screen, and the two pieces of gold consume the wire simultaneously from opposite ends, finally agglomerating into a single stationary nanoparticle. In Figure 1e, the particle encounters a junction of crossed wires and has the option of continuing along the initial wire or switching to a different wire; after proceeding a short distance into the new wire it switches back to the initial path until reaching a final stop. The TEM heating substrates used (Protochips Aduro platform) are composed of a thick ceramic which acts as the heater, containing a regular array of 7-μm-diameter holes and a carbon support film overlay. Due to the thickness of the ceramic, high quality TEM images are attainable only on those areas of carbon overlaying a hole in the ceramic. For this reason, should the catalyst particle migrate over the edge of a hole onto the ceramic heater, the experiment was terminated, as occurs at the end of Movie S5 (Figure 1e last panel).

The rate of the reverse VLS mechanism was controlled by varying the temperature, using higher temperatures to increase the rate at which the catalyst particle migrates the length of the wire, and removing the heat to effectively and instantaneously prevent further motion of the particle. This ability to repeatedly quench and restart the wire dissolution process was utilized to collect compositional data at intervals during the experiment, by performing energy dispersive X-ray spectroscopy (EDS) on the gold catalyst particle. EDS spectra were collected intermittently by periodically quenching the system to room temperature to stop the motion of the nanoparticle and collect the spectrum, subsequently returning to the original experimental

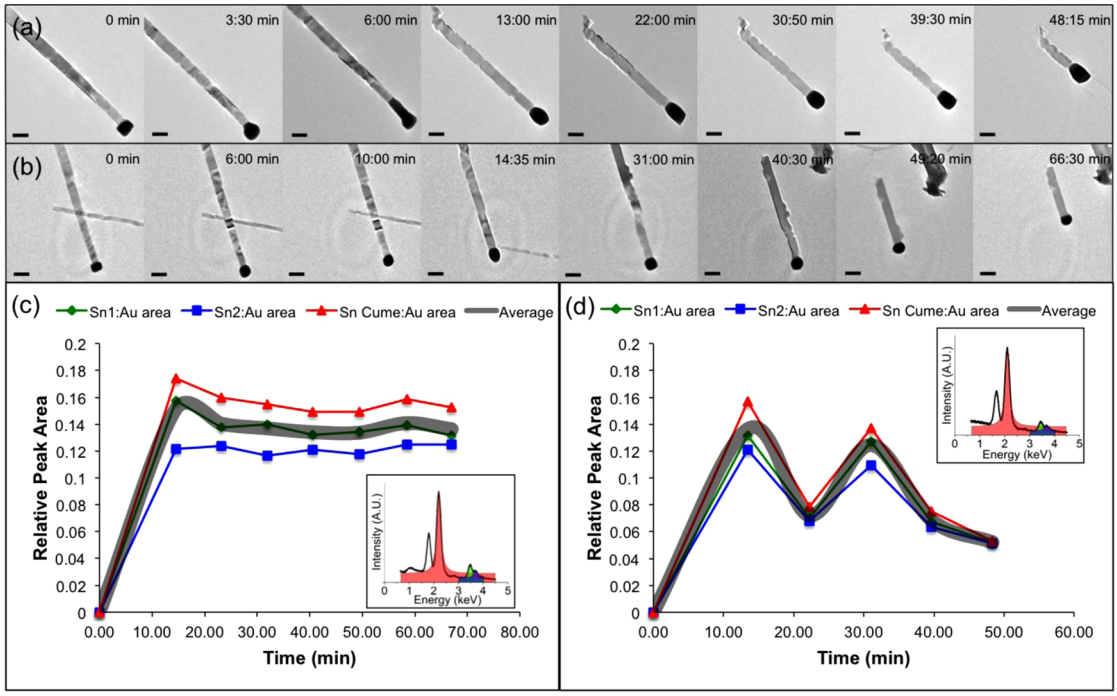

Figure 2. ***In situ*** **compositional analysis of two SnO_2 nanowires (corresponding to Movies S6–S7). (a and b) Images extracted from movies of nanowire heating. Scale bars are 100 nm. (c and d) Relative EDS peak areas as a function of time taken from wires (a and b), respectively. Insets: Representative EDS spectra. Shaded regions indicate integrated area from Voigt fitting. Gold peak is shaded in red, Sn1 in green, and Sn2 in blue. The peak at 1.7 keV is Si from the substrate. Wires were heated to 700 °C and quenched in 8.5 min intervals to stop droplet movement and acquire EDS spectra.**

temperature once a spectrum had been collected. To compare multiple sets of data, we performed systematic EDS collection from pure SnO_2 nanowires using a standard procedure, ramping the temperature at 2 °C/s from room temperature until 700 °C, holding the wire at 700 °C during dissolution, and quenching and taking spectra at intervals of 8.5 min. Figure 2 shows EDS spectra acquired from two wires using this procedure. The Sn Lα and Lβ peaks at 3.4 and 3.6 keV and the Au Mα peak at 2.1 keV were fit to Voigt functions, and the area under the curve was found for each peak in each spectrum. Frames from the movies of the two wires taken between EDS collection times are shown in Figure 2a,b. Plotted in Figure 2c,d are the relative ratios of the integrated intensity of the Sn and Au peaks at each time during the EDS data collection. Full movies are available in the Supporting Information movie files, Movies S6–S7.

Initially, before heating, no Sn is detected in the catalyst particle at the wire head. After several minutes of nanoparticle migration, however, Sn Lα and Lβ peaks appear indicating the presence of Sn in the metal tip. After the initial spike in Sn concentration, the ratio of Sn/Au falls, and though fluctuating throughout the remainder of the experiment, it appears to reach a relatively steady state. Though qualitative in nature, these observations show that the steps of the VLS mechanism appear to be occurring in reverse. First, the Au droplet melts, at a temperature much closer to the Sn–Au liquidus temperature of 483 °C

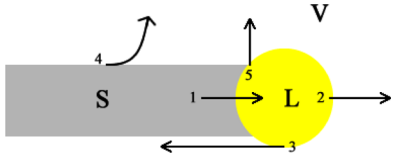

Figure 3. Cartoon depicting the five processes taking place during SLV dissolution of the nanowire: (1) SnO_2 dissolves into Au droplet at SL interface. (2) Sn is ejected at the LV interface. (3) Adhesion between droplet and substrate is overcome so that the dissolution and ejection steps can maintain a steady state. (4) SnO_2 vaporization from nanowire sidewall (SV interface). (5) Possible evaporation of O at the SLV triple junction.

than that of bulk gold (1084 °C),[34] implying an initial diffusion of Sn into the Au droplet to form an alloy. Next, the SnO_2 dissolves in the droplet causing a spike in the Sn/Au ratio in an incorporation step, which is the reverse of the initial crystallization. Finally, the Au–Sn alloy reaches a supersaturation and Sn is ejected from the droplet, presumably by evaporation, although some surface diffusion cannot be ruled out. One additional step in this SLV type process is that in order for the droplet to continue to incorporate Sn, so that the dissolution and evaporation steps may retain a steady state, it must overcome adhesion to the substrate surface so that it is mobile. These mechanistic steps are indicated schematically in Figure 3.

Though EDS clearly shows that the Sn dissolves from the wire into the droplet and is ejected, it is not clear from EDS whether the oxygen content of the wire is

lost entirely at the liquid−vapor interface, or if dissociative dissolution of SnO_2 to SnO and O (as would be expected) occurs at the solid−liquid interface, allowing some oxygen to evaporate at the triple junction, since the spectrometer used for *in situ* EDS collection did not have sufficient resolution to resolve the oxygen peak.

Several aspects of the qualitative observations described above provide clues regarding the growth mechanism for this system. First, a comparison of Figure 1, panels a and b, shows that wire dissolution can occur either *via* a layer-by-layer mechanism, thereby maintaining the wire diameter, or directly at the solid−vapor interface, resulting in a continuous reduction in wire diameter. To study the kinetics of SLV nanowire dissolution, we performed a systematic dissolution of 19 nanowires using the same heating procedure: the substrate temperature was initially stepped directly to 450 °C, then ramped to 750 °C at a rate of 0.2 °C/s, and then held at 750 °C while recording the rate of wire dissolution. In all cases, the particle melted and began to move at a temperature between 450 and 750 °C, and these temperatures were recorded. The data for all 19 wires is given in Chart S1 in Supporting Information. Of the 19 wires, 15 were single-crystalline and used for further analysis. While a slight dependence of melting temperature, T_{melt}, on droplet diameter, d_{drop} is observed as expected, interestingly, no dependence on wire diameter, d_{wire}, is observed for either T_{melt}, or the temperature at which the droplet is first seen to move, T_{move} (Figures S2−S4a,b). Additionally, there is no observed dependence of the rate of dissolution, dL/dt, on either d_{wire} or the ratio of droplet to wire diameters, d_{drop}/d_{wire}. (Figures S2−S4c,d), though a lot of scatter is seen in all of these plots. This observation that the rate of dissolution is independent of wire diameter suggests that SLV dissolution is not occurring in a mechanistic regime dominated by the Gibbs−Thomson criterion, similar to the *in situ* growth observations of Kodambaka *et al.*[23] This suggests that the ejection of Sn at the LV interface is either a key step in the mechanism or at least as dominant as incorporation of Sn into the droplet by dissolution.

For the 15 wires which underwent analysis, they were first separated into two groups, of 10 wires which underwent typical SLV dissolution of the wire with no noticeable change in diameter, and five wires which underwent simultaneous thinning of the wire, reducing its diameter as is seen in Figure 1b. For the group which showed simultaneous wire thinning as well as SLV dissolution, it is difficult to observe trends in T_{move}, T_{melt}, or dL/dt, with wire or droplet diameters. This is probably due to both the small sample size, and because multiple mechanistic steps are simultaneously occurring. We speculate that wires which acquired a Au coating during synthesis, as described by Hannon *et al.*,[27] may undergo Au-catalyzed dissolution simultaneously through the nanowire sidewalls and through the droplet at the tip. Though this is difficult to verify directly, those wires with considerable wetting of the sidewalls from the catalyst droplet should have smaller d_{drop}/d_{wire} ratios than those with Au confined at the tip, and this is consistent with an average d_{drop}/d_{wire} value of 1.397 ± 0.214 nm for the group which underwent thinning, in comparison to an average d_{drop}/d_{wire} value of 1.640 ± 0.212 nm for the group which did not.[27]

For those wires which predominantly underwent SLV dissolution (with no thinning), it was necessary for the catalyst droplet to overcome initial adhesion and maintain continuous mobility, so that the wire could continuously dissolve in the particle. Not doing so resulted in the droplet and nanowire disconnecting, which terminated the nanowire dissolution. On the assumption that the droplet velocity has an Arrhenius dependence on temperature, and that the particle must have some initial critical velocity for movement to be observed, we conclude that the activation energy associated with overcoming adhesion must be proportional to our observed T_{move}. Furthermore, this energy should also be proportional to the contact area between the droplet and the substrate surface, which itself is roughly proportional to the cross-sectional area of the droplet. To test this hypothesis, we plotted T_{move} as a function of d_{drop}^2, and a rough proportionality is observed (Figure 4a), though admittedly with some scatter. Shown in Figure 4b is a plot of dissolution rate, dL/dt, with T_{move}. Despite the scatter in the data, it is clear that high values of T_{move} do not occur simultaneously with high dissolution rates, as might be expected if there is a strong adhesive force inhibiting droplet mobility.

The temperature dependence of dL/dt is shown in Figure 4c. These plots were measured from movies of two wires in which dissolution was observed for several minutes at a time at different growth temperatures. Assuming Arrhenius behavior and using a least-squares analysis to make a linear fit to both sets of data, we obtain activation energies for the SLV dissolution of the two SnO_2 nanowires of 0.89 and 1.07 eV, respectively. These values are similar in order of magnitude to values found for the VLS growth of Si nanowires,[27] and are substantially smaller than the enthalpy of dissociative vaporization of SnO_2 from an uncatalyzed surface, reported to be 4.3 eV.[35]

An additional factor which may be at play during this process is the size-dependent composition of the catalyst droplets reported by Sutter and Sutter.[29] They find for Au-catalyzed Ge nanowire growth, that the smaller the catalyst droplet, the greater the concentration of Ge, enabling them to controllably suppress the liquidus. If a similar mechanism is at play in these systems, then the smaller catalyst droplets will incorporate a greater concentration of Sn, translating to higher levels of supersaturation and faster dL/dt. A plot of dL/dt

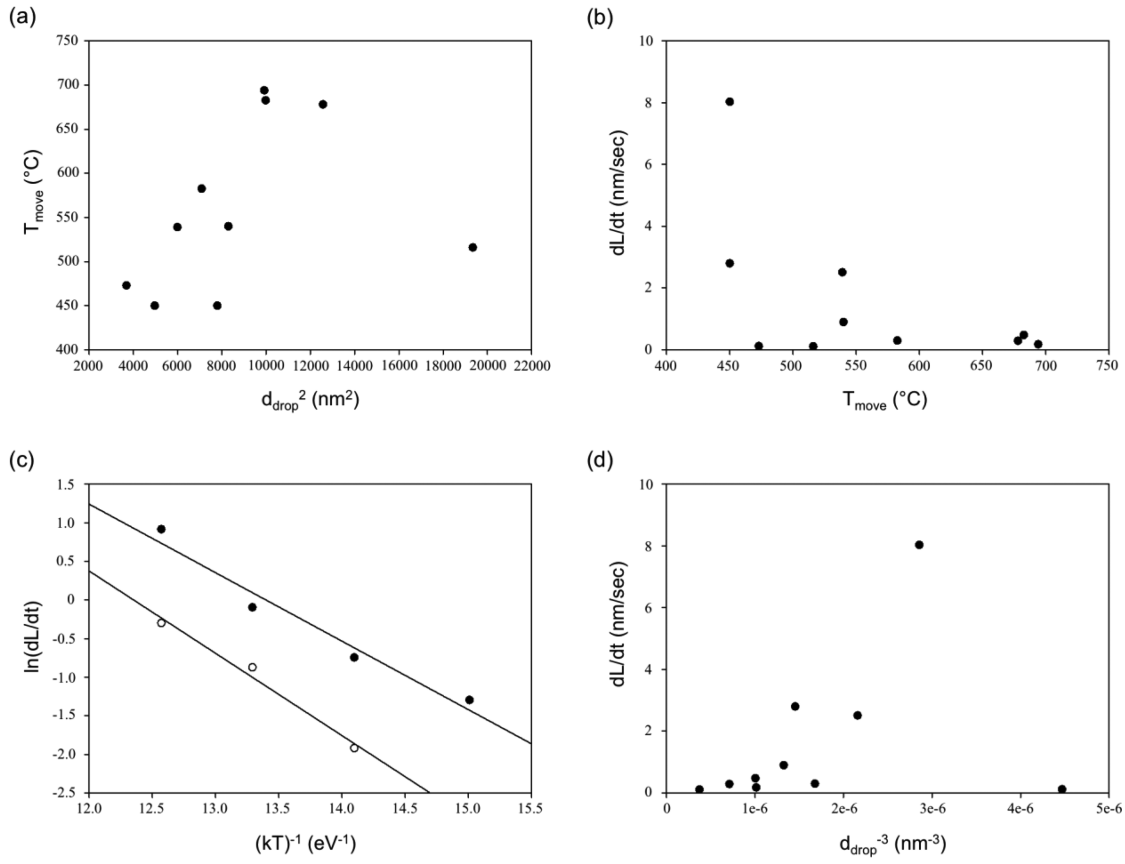

Figure 4. Kinetics of Au-catalyzed SnO_2 nanowire dissolution. (a, b, and d) Nanowires were heated from 450 to 750 °C at 0.2 °C/s, and then annealed at 750 °C while dissolution rate was measured. All wires were single-crystalline and underwent dissolution into the droplet with no observable change in wire diameter. (a) Temperature at which droplet is first observed to move, T_{move}, as a function of the square of droplet diameter. (b) Dissolution rate as a function of T_{move}. (c) Arrhenius plot of dissolution rate as a function of 1/*T*, for two nanowires, yielding activation energies of 0.89 eV (closed circles) and 1.07 eV (open circles). (d) Dissolution rate as a function of 1/droplet volume.

versus $1/d_{drop}^3$ (Figure 4d) shows a rough proportionality consistent with this scenario.

To measure the pressure dependence of the SnO_2 dissolution, we conducted a series of annealing experiments (Figure 5 table) in which we annealed as-grown scanning electron microscope (SEM) substrates in a CVD furnace, to control the atmosphere and pressure between 2 and 500 Torr, which is representative of the entire pressure range available to us with controlled atmosphere. Oxygen mole fraction was varied between 0 and 1, with the remaining pressure exerted by Ar. For each annealing experiment, 100 sccm of gas was used in total. On annealing with the minimum total pressure and minimum oxygen partial pressure (2 Torr and 0, respectively) at 700 °C, no change in the wire appearance was observable under SEM (Figure 5 a). Increasing the temperature to 900 °C also saw no change, but degradation to the wires was observed at 1000 °C, with noticeably fewer wires present, and those remaining having no observable catalyst tip (Figure 5b). Performing the same experiment but with greater mole fractions of oxygen also led to the same level of wire degradation, suggesting that total pressure, rather than oxygen partial pressure, is more dominant in the vaporization of SnO_2. Two further experiments were conducted at atmospheric pressure, annealing a TEM Protochips substrate with SnO_2 nanowires deposited upon it. In these experiments, annealing in atmospheric oxygen resulted in no observable change, but a slight degradation of the wires can be observed after annealing in an oxygen-free environment. In these experiments, the catalyst tip is still observable, but the wire morphology is no longer perfectly straight. While definitive conclusions would require us to be able to control the atmosphere while tuning the pressure between the 2 Torr available to us using the CVD furnace, and the 10^{-6} Torr of the TEM column, it is clear from these results that Au-catalyzed dissolution of the wires is highly dependent on pressure, requiring low pressure for the reproducible dissolution of entire wires. We speculate that the slight dependence of wire degradation on oxygen partial pressure is indicative of a secondary, much slower, vaporization directly from the nanowire sidewalls. This conclusion is consistent with the findings of Klamchuen *et al.*, who found that a dependence of SnO_2 nanowire growth on oxygen partial pressure was indicative of competing mechanisms at the SV and LV interfaces.[36]

P_{total} (Torr)	X_{Oxygen}	T (°C)	T (min)	Results
2	0	700	30	No change
2	0	900	30	No change
2	0	1000	30	Degradation
2	0.67	1000	30	Degradation
2	1	1000	30	Degradation
500	1	700	30	No change
760	0	700	60	Small degradation
760	0.22	700	60	No change

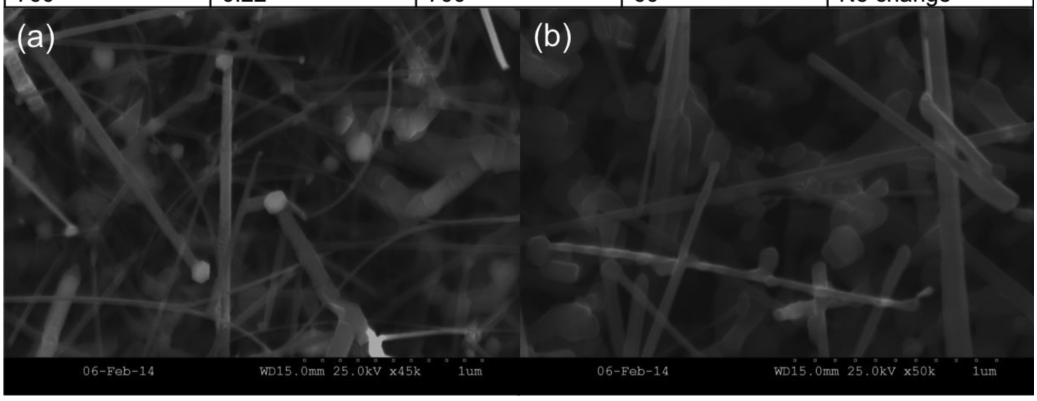

Figure 5. Pressure dependence of SnO_2 nanowire dissolution. Table: parameters used for annealing experiments. (a) SnO_2 as-grown nanowires imaged by SEM; (b) SnO_2 nanowires annealed at $P_{total} = 2$ Torr, $X_{oxygen} = 1$, $T = 1000$ °C. Gold droplets are no longer present and density of wires is reduced, indicating wire degradation.

CONCLUSIONS

In conclusion, the combination of kinetic studies showing the correlation of T_{move} with catalyst droplet area and dissolution rate with droplet volume, the observed lack of dependence of dissolution rate on wire diameter, and the low pressures necessary for observable wire dissolution allow us to consistently explain our observations in terms of SLV dissolution of our nanowires, dependent on two crucial steps: (1) the ability of the catalyst droplet to overcome adhesion to the substrate, such that a steady state may be reached between Sn incorporation and ejection, and (2) the evaporation of the wire from the LV interface. The method outlined herein should provide an experimental platform to explore several features relevant to the VLS growth mechanism, such as the saturation concentration of a reactant within a VLS catalyst droplet and the use of VLS catalyst metals for the controlled etching of semiconducting materials.

METHODS

The nanowires were prepared using a VLS synthesis from the literature.[37] Before starting the VLS synthesis, a silicon substrate was coated in a 20 nm layer of Au deposited by electron beam evaporation. Pure SnO_2 nanowires were grown by mixing SnO (Alfa Aesar, purity, 99.996%) and graphite (Alfa Aesar, purity, 99.9995%) powders in a 1:1 molar ratio, and placing the mixture in a quartz tube about 5 in. upstream from a silicon substrate, all contained within a CVD furnace. The system was pumped to 1.7 Torr under 100 sccm of flowing argon, heated to 950 °C at 20 °C/min, and held at that temperature for 30 min. In-doped SnO_2 nanowires were prepared under the same reaction conditions using a 4:1:1 molar ratio of In_2O_3 (Alfa Aesar, purity, 99.99%)/SnO/graphite.

Nanowires were characterized using XRD (Bruker D8 Advanced and Bruker D8 Discover with Cu Kα radiation), SEM (Hitachi S-4300), TEM (JEOL 2010F at 200 keV and Hitachi HF-3300 at 300 keV), and EDS (Oxford INCA detector). *In situ* heating was performed using a Protochips Aduro heating stage, and Camtasia screen recording software was used to record videos. TEM samples were prepared by sonication of the as-grown substrates in methanol, followed by dropcasting onto the relevant commercial substrate—lacey carbon coated copper for TEM imaging, or a Protochips Aduro thermal "E-chip" for *in situ* TEM heating experiments. The Protochips E-chip comprises a 300 μm × 300 μm ceramic substrate which acts as both sample support and heater. As such, temperature changes are virtually instantaneous, resulting in isothermal conditions across the entire supported sample.

Conflict of Interest: The authors declare no competing financial interest.

Acknowledgment. This research was supported by the NASA Kentucky Space Program (B.M.H.), the NASA Kentucky EPSCoR Program (Y.-J.C. and B.S.G.), the Office of Basic Energy Sciences, Materials Sciences and Engineering Division, U.S. Department of Energy (B.S.G.), partially supported by the Kentucky NSF EPSCoR program through the Center of Advanced Materials, and in part by ORNL's Center for Nanophase Materials Sciences (CNMS), which is sponsored by the Scientific User Facilities Division, Office of Basic Energy Sciences, U.S. Department of Energy.

Supporting Information Available: XRD and scanning transmission electron microscope (STEM) data for nanowire

characterization (Figure S1); chart of 19 wires heated under same heating profile (Chart S1); plots of nanowire kinetics for 15 single-crystalline nanowires (Figure S2); plots of nanowire kinetics for 10 single-crystalline nanowires that did not thin during heating (Figure S3); plots of nanowire kinetics for five single-crystalline nanowires that did thin during heating (Figure S4); movies S1–S7. This material is available free of charge *via* the Internet at http://pubs.acs.org.

REFERENCES AND NOTES

1. Wagner, R. S.; Ellis, W. C. Vapor-Liquid-Solid Mechanism of Single Crystal Growth. *Appl. Phys. Lett.* **1964**, *4*, 89–90.
2. Wu, Y.; Yang, P. Direct Observation of Vapor–Liquid–Solid Nanowire Growth. *J. Am. Chem. Soc.* **2001**, *123*, 3165–3166.
3. Lu, W.; Lieber, C. M. Semiconductor Nanowires. *J. Phys. Appl. Phys.* **2006**, *39*, R387.
4. Cui, Y.; Wei, Q.; Park, H.; Lieber, C. M. Nanowire Nanosensors for Highly Sensitive and Selective Detection of Biological and Chemical Species. *Science* **2001**, *293*, 1289–1292.
5. Kolmakov, A.; Zhang, Y.; Cheng, G.; Moskovits, M. Detection of CO and O_2 Using Tin Oxide Nanowire Sensors. *Adv. Mater.* **2003**, *15*, 997–1000.
6. Yu, C.; Hao, Q.; Saha, S.; Shi, L.; Kong, X.; Wang, Z. L. Integration of Metal Oxide Nanobelts with Microsystems for Nerve Agent Detection. *Appl. Phys. Lett.* **2005**, *86*, 063101.
7. Baxter, J. B.; Aydil, E. S. Nanowire-Based Dye-Sensitized Solar Cells. *Appl. Phys. Lett.* **2005**, *86*, 053114–053114–3.
8. Gubbala, S.; Chakrapani, V.; Kumar, V.; Sunkara, M. K. Band-Edge Engineered Hybrid Structures for Dye-Sensitized Solar Cells Based on SnO_2 Nanowires. *Adv. Funct. Mater.* **2008**, *18*, 2411–2418.
9. Krishnamoorthy, T.; Tang, M. Z.; Verma, A.; Nair, A. S.; Pliszka, D.; Mhaisalkar, S. G.; Ramakrishna, S. A Facile Route to Vertically Aligned Electrospun SnO2 Nanowires on a Transparent Conducting Oxide Substrate for Dye-Sensitized Solar Cells. *J. Mater. Chem.* **2012**, *22*, 2166.
10. Duan, X.; Huang, Y.; Cui, Y.; Wang, J.; Lieber, C. M. Indium Phosphide Nanowires as Building Blocks for Nanoscale Electronic and Optoelectronic Devices. *Nature* **2001**, *409*, 66–69.
11. Cui, Y.; Zhong, Z.; Wang, D.; Wang, W. U.; Lieber, C. M. High Performance Silicon Nanowire Field Effect Transistors. *Nano Lett.* **2003**, *3*, 149–152.
12. Park, M.-S.; Wang, G.-X.; Kang, Y.-M.; Wexler, D.; Dou, S.-X. Liu. Preparation and Electrochemical Properties of SnO2 Nanowires for Application in Lithium-Ion Batteries. *Angew. Chem., Int. Ed.* **2007**, 750–753.
13. Ko, Y.-D.; Kang, J.-G.; Park, J.-G.; Lee, S.; Kim, D.-W. Self-Supported SnO_2 Nanowire Electrodes for High-Power Lithium-Ion Batteries. *Nanotechnology* **2009**, *20*, 455701.
14. Chueh, Y.-L.; Ko, M.-T.; Chou, L.-J.; Chen, L.-J.; Wu, C.-S.; Chen, C.-D. $TaSi_2$ Nanowires: A Potential Field Emitter and Interconnect. *Nano Lett.* **2006**, *6*, 1637–1644.
15. Kaur, J.; Kumar, R.; Bhatnagar, M. C. Effect of Indium-Doped SnO_2 Nanoparticles on NO_2 Gas Sensing Properties. *Sens. Actuators, B* **2007**, *126*, 478–484.
16. Salehi, A.; Gholizade, M. Gas-Sensing Properties of Indium-Doped SnO_2 Thin Films with Variations in Indium Concentration. *Sens. Actuators, B* **2003**, *89*, 173–179.
17. Salehi, A. Selectivity Enhancement of Indium-Doped SnO_2 Gas Sensors. *Thin Solid Films* **2002**, *416*, 260–263.
18. Gao, J.; Chen, R.; Li, D. H.; Jiang, L.; Ye, J. C.; Ma, X. C.; Chen, X. D.; Xiong, Q. H.; Sun, H. D.; Wu, T. UV Light Emitting Transparent Conducting Tin-Doped Indium Oxide (ITO) Nanowires. *Nanotechnology* **2011**, *22*, 195706.
19. Wang, D.; Chen, G.; Gong, M. Effects of Indium Doping Concentration on the Morphology and Electrical Properties of One-Dimensional SnO_2 Nanostructures Prepared by a Molten Salt Method. *Sci. China: Phys., Mech. Astron.* **2012**, *55*, 1599–1603.
20. Schmidt, V.; Wittemann, J. V.; Senz, S.; Gösele, U. Silicon Nanowires: A Review on Aspects of Their Growth and Their Electrical Properties. *Adv. Mater.* **2009**, *21*, 2681–2702.
21. Schmidt, V.; Wittemann, J. V.; Gösele, U. Growth, Thermodynamics, and Electrical Properties of Silicon Nanowires†. *Chem. Rev.* **2010**, *110*, 361–388.
22. Givargizov, E. I. Fundamental Aspects of VLS Growth. *J. Cryst. Growth* **1975**, *31*, 20–30.
23. Kodambaka, S.; Tersoff, J.; Reuter, M. C.; Ross, F. M. Diameter-Independent Kinetics in the Vapor-Liquid-Solid Growth of Si Nanowires. *Phys. Rev. Lett.* **2006**, *96*, 096105.
24. Roper, S. M.; Davis, S. H.; Norris, S. A.; Golovin, A. A.; Voorhees, P. W.; Weiss, M. Steady Growth of Nanowires *via* the Vapor-Liquid-Solid Method. *J. Appl. Phys.* **2007**, *102*, 034304.
25. Ryu, S.; Cai, W. Molecular Dynamics Simulations of Gold-Catalyzed Growth of Silicon Bulk Crystals and Nanowires. *J. Mater. Res.* **2011**, *26*, 2199–2206.
26. Wang, H.; Zepeda-Ruiz, L. A.; Gilmer, G. H.; Upmanyu, M. Atomistics of Vapour–Liquid–Solid Nanowire Growth. *Nat. Commun.* **2013**, *4*, No. 1956.
27. Hannon, J. B.; Kodambaka, S.; Ross, F. M.; Tromp, R. M. The Influence of the Surface Migration of Gold on the Growth of Silicon Nanowires. *Nature* **2006**, *440*, 69–71.
28. Sutter, E.; Sutter, P. Au-Induced Encapsulation of Ge Nanowires in Protective C Shells. *Adv. Mater.* **2006**, *18*, 2583–2588.
29. Sutter, E. A.; Sutter, P. W. Size-Dependent Phase Diagram of Nanoscale Alloy Drops Used in Vapor–Liquid–Solid Growth of Semiconductor Nanowires. *ACS Nano* **2010**, *4*, 4943–4947.
30. Sutter, E.; Sutter, P. Formation and Stabilization of Single-Crystalline Metastable AuGe Phases in Ge Nanowires. *Nanotechnology* **2011**, *22*, 295605.
31. Sutter, E. A.; Sutter, P. W.; Uccelli, E. Fontcuberta i Morral, A. Supercooling of Nanoscale Ga Drops with Controlled Impurity Levels. *Phys. Rev. B* **2011**, *84*, 193303.
32. Givargizov, E. I.; Babasiam, P. A. Negative Whiskers Formed by Solid-Liquid-Vapor Mechanism during Vaporization of ZnS. *J. Cryst. Growth* **1977**, *37*, 140–146.
33. Kim, B.-J.; Stach, E. A. Desorption Induced Formation of Negative Nanowires in GaN. *J. Cryst. Growth* **2011**, *324*, 119–123.
34. Okamoto, H.; Massalski, T. B. The Au–Sn (Gold-Tin) System. *Bull. Alloy Phase Diagrams* **1984**, *5*, 492–503.
35. L'vov, B. V.; Brown, M. E. Sublimation and Decomposition Reactions. In *Thermal Decomposition of Solids and Melts*; Hot Topics in Thermal Analysis and Calorimetry; Springer: The Netherlands, 2007; pp 163–228.
36. Klamchuen, A.; Yanagida, T.; Kanai, M.; Nagashima, K.; Oka, K.; Kawai, T.; Suzuki, M.; Hidaka, Y.; Kai, S. Role of Surrounding Oxygen on Oxide Nanowire Growth. *Appl. Phys. Lett.* **2010**, *97*, 073114.
37. Kim, H.; Park, S.; Jin, C.; Lee, C. Enhanced Photoluminescence in Au-Embedded ITO Nanowires. *ACS Appl. Mater. Interfaces* **2011**, *3*, 4677–4681.